Journal of Food Measurement and Characterization (2023) 17:2313–2325
https://doi.org/10.1007/s11694-022-01793-5

ORIGINAL PAPER

Rapid detection of gingerol and thymol in medicinal foods based on Fe_2O_3 nanoparticles modified glassy carbon electrode

G. Veerapandi[1] · S. Meenakshi[1] · C. Sekar[1]

Received: 14 April 2022 / Accepted: 19 December 2022 / Published online: 31 December 2022

Abstract

Ginger and Ajwain are used extensively in food products, natural medicine to treat certain common diseases and as an immunity booster against viral infections. In this work, we report the fabrication of a novel electrochemical sensor based on α-Fe_2O_3 nanoparticles for detection and quantification of [6]-Gingerol (GIN) and Thymol (THY) which are water soluble phytochemicals derived from edible herbs Ginger and Ajwain respectively. The α-Fe_2O_3 nanoparticles were synthesised by sol-gel method and its structure and composition were confirmed by powder X-ray diffraction and photoelectron spectroscopy studies. The α-Fe_2O_3 NPs modified glassy carbon electrode (GCE) exhibited an excellent electrocatalytic activity towards the oxidation of GIN and THY in phosphate buffer saline at pH 7. The α-Fe_2O_3 modified GCE exhibited the lowest detection limits of 35.2 nM and 24 nM for GIN and THY respectively over the corresponding dynamic ranges of 55.6 nM to 118 µM and 27.8 nM to 56 µM. Detailed interference study confirmed the potential anti-interference ability of the fabricated sensor against a number of potential interfering compounds. Cyclic stability study yielded relative standard deviation (RSD) values of 9.9% and 9.18% for GIN and THY respectively, demonstrating excellent stability of the sensor. Reproducibility of the α-Fe_2O_3/GCE was investigated by testing a number of electrodes which yielded RSD values of 1.08% and 0.97%, for GIN and THY respectively. These promising characteristic features of the proposed sensor make it suitable for quick and precise detection of GIN and THY in food and natural medicines.

Graphical Abstract

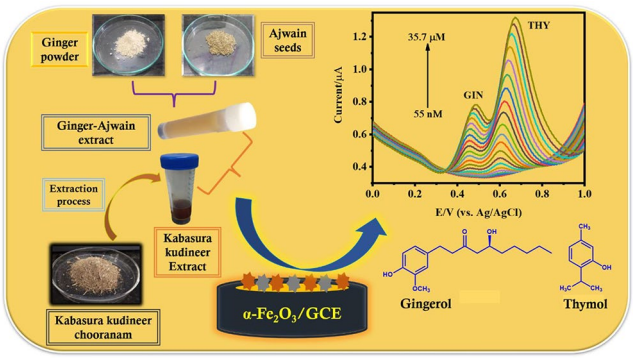

Keywords Food sensors · Medicinal herbs · Gingerol · Thymol · Kabasura Kudineer

GV and SM equally contributed to this paper.

1. Introduction

Ginger, a flowering plant originated from Southeast Asia, is used in traditional food items of India, China, and around the world. Rhizome part of the ginger is commonly used as spice and it is known to contain many nutrients and bioactive compounds including Zingerones, Shogaols, and Gingerols[1] that have powerful benefits for human body and brain. Among these, 6-Gingerol or Gingerol ($C_{17}H_{26}O_4$) has many attractive properties of pharmacological importance[1–3]. Gingerol forms as yellow colored powder with a low melting point of 30 to 32 °C having pungent odor[4]. It has anti-inflammatory[2, 3], anti-oxidant[2, 5], anti-tumor[5], anti-apoptotic[6],and anti-bacterial properties. High pressure liquid chromatography(HPLC)[7] and spectroscopic techniques (Ultraviolet-visible) have been employed to determine 6-gingerol in ginger extract, and foods. Though electrochemical sensors are gaining popularity for detection and quantification of several analytes because of its simplicity, low-cost, high sensitivity, and selectivity, there exists only one report dealing with the detection of gingerol. Chaisiwamongkholet al. reported the fabrication of an electrochemical sensor for detecting gingerol spices in ginger using multiwalled carbon nanotubes (MWCNT) modified basal plane pyrolytic graphite electrode[3].The authors used anodic stripping voltammetry to quantify gingerol over a narrow dynamic range of 1 to 50 µM with the lowest detection limit of 0.21 µM.

Ajwain caraway or bishop's weed, is a spice derived from an herb plant in the *Apiaceae* family. The seeds have a bitter and pungent flavour, like oregano. Ajwain is often added to several food items because of its strong aromatic essence and rich fibre, minerals and vitamins content. Ajwain is the major source of Thyme oil, from which Thymol (2-isopropyl-5-methylphenol), a colourless crystalline monoterpene phenol is extracted. In addition to its use as dietary item, thymol is extensively used as antiseptic lotions, mouth wash liquids, inhalation mixtures, perfumes, and food additive[8, 9]. Thymol has been widely used for centuries as traditional medicine due to its pharmacological properties such as antibacterial, anti-fungal, anti-oxidative and anti-inflammatory properties[10]. It is fed to pigs along with cinnamaldehyde to improve their immune system by increasing the levels of immunoglobulins (IgA/IgM) in their gut[9]. Despite such potential applications of thymol, very few electrochemical sensors based on CeO_2/GN/GCE[8], CeO_2/Brij35/GCE[11], and single walled carbon nanotubes modified screen printed electrodes (SWCNT/SPE)[12] have been reported for the determination of Thymol. Hence, there is a need for development of a simple and efficient sensor for the detection of GIN and THY.

The physical and chemical properties of metal oxide nanostructures are known to depend on several design parameters such as particle size, morphology, interparticle distances and the dielectric constant of the surrounding medium. Moreover, the metal oxide nanostructures exhibit several unique features such as functional biocompatibility, biosafety, chemical stability and improved catalytic properties which are essential characteristics for various applications such as fuel cell[13], energy storage[14, 15], and sensors[16–19]. In particular, the advent of nanomaterials enabled the discovery of a number of electrochemical sensors with high performance.

Electrochemical sensors continue to be an attractive analytical tool because of its unique features such as high sensitivity, low cost, ease of use, and less sample quantity requirement for analysis. Numerous electrochemical sensors are used in food industry to monitor quality at each stage starting from production to consumer level. The presence and amounts of heavy metals, pathogens, colouring agents, preservatives, and pesticides must be monitored regularly in order to ensure food quality. Nasehi et al. fabricated an electrochemical sensor using TiO_2-SWCNTs and 1-hexyl 3-methyl imidazolium hexafluorophosphate as electrode material for monitoring Bisphenol-A in water and soft drinks[19]. Buledi et al. developed an electrochemical sensor based on WO_3-rGO nanocomposite for determining 'mancozeb', a biocide, in vegetables and fruits[18]. Anithaa et al. fabricated a non-enzymatic electrochemical sensor based on WO_3 nanoparticles for the determination of histamine in vinegar sample[20]. In another report, the same author has developed a sensor based on UV-rays irradiated WO_3 nanoparticles for determining tyrosine and tryptophan in milk and egg samples[21]. Veerapandi et al. has reported HAP-TiO_2 nanocomposite based electrochemical sensor for ascorbic acid and eugenol detection in fruit juice and herbal medicine[22]. Lavanya et al. determined vitamins such as ascorbic acid and folic acid using Mn doped SnO_2 nanoparticles based electrochemical sensor[23]. Meenakshi et al. have used shock wave irradiated Fe_2O_3 nanoparticles for the determination of riboflavin and folic acid[24].

Among several metal oxides, Fe_2O_3 has received much attention due to its diverse physiochemical properties and it is used in a wide range of technological applications. It is naturally available in abundance, inexpensive, environmental friendly, non-toxic, and biocompatible. Iron is found in a variety of foods, including dark chocolate, red meat, seafood, beans, spinach, and apricots. Furthermore, the human body requires iron for growth and development, and it is used by our body to produce haemoglobin and myoglobin [25]. In addition, several researchers have reported

the enzyme like activity of α-Fe_2O_3[26]. These unique properties of Fe_2O_3 make it an attractive material for sensing applications.

In this work, we report the fabrication of α-Fe_2O_3 nanoparticles based electrochemical sensor for the detection of Gingerol in ginger (Zingiber officinale) and Thymol in ajwain (Anisochilus carnosus) extracts. The developed electrode exhibited an excellent electrocatalytic activity towards the oxidations of gingerol and thymol over wider linear ranges and significantly high limit of detection (LOD) values which are sufficient for the intended food control applications. The fabricated electrode selectively detects precise amounts of gingerol and thymol in presence of a number of phytocompounds and minerals which are present in Kabasura Kudineer (KsK), a decoction derived by boiling a mixture of 15 different dried herbs in water. In southern part of India, this decoction containing Zingiber officinale (Ginger) and Thymus Vulgaris (Ajwain), among others, has been extensively used as an immunity booster against viral infections including COVID-19.

2. Materials and methods

2.1 Reagents and apparatus used

Iron nitrate ($Fe(NO_3)_2.9H_2O$) (98%, CAS No. 7782-61-8) and Disodium hydrogen phosphate (Na_2HPO_4)(99%, CAS No. 10028-24-7) were purchased from Merck specialities. Sodium dihydrogen phosphate (NaH_2PO_4) (99%, CAS No. 13472-35-0) and Sodium hydroxide (NaOH) (97%, CAS No. 1310-73-2) pellets were purchased from Spectrochem and Thermo Fisher Scientific respectively. Gingerol (98%, CAS No. 23513-14-6) and Thymol (99%, CAS No. 89-83-8) were purchased from TCI chemicals. All analytical reagent grade chemicals were used as received without further purification. Deionized water produced by ultrapurification system was used in all the experiments. Powder X-ray diffraction (XRD) measurements were recorded using X'Pert Pro PANalytic. High resolution transmission electron microscope (HRTEM; JEOL JEM 2100) was for microstructural investigation of Fe_2O_3 nanoparticles. Electrochemical measurements were carried out on CHI 608D electrochemical workstation. In the three-electrode cell, working electrodes were prepared by modifying glassy carbon electrode (GCE), commercial electrodes Ag/AgCl and platinum wire were used as reference and counter electrodes. Electrochemical impedance spectroscopy (EIS) measurements were made (ac potential 5 mV; dc potential 250mV) in the frequency range 100 kHz to 1 Hz in 1 M KCl containing 1.0 mM $[Fe(CN)_6]^{3-/4-}$ redox couple. The impedance data were presented in the form of Nyquist plots and the charge transfer resistance (R_{CT}) was determined using ZSimpWin software simulations.

2.2 Preparation of α-Fe_2O_3 /GCE

α-Fe_2O_3 nanoparticles was synthesized by sol-gel method. Precursor solution was prepared by dissolving 0.1 M $Fe(NO_3).9H_2O$ in 200 mL deionised water and it was added drop wise under vigorous stirring with aqueous solution of 0.2 M monohydrated citric acid. The mixed solution was heated at 70 °C until gel was formed and water was evaporated. Then, the prepared sample was washed 10 times using distilled water and dried in hot air oven at 100 °C for 2 h. The dried powder was annealed at 700 °C for 3 h in ambient atmosphere.

Glassy carbon electrodes (3 mm diameter) were polished with the 0.3 μm alumina slurry and cleaned surfaces were sonicated in ethanol-water mixture to remove unwanted microscopic dust particles. 10 μL of supernatant dispersed (1 mg α-Fe_2O_3 per 1mL) in demineralised water was drop-casted on glassy carbon electrode (GCE; 3 mm) surface, and dried at room temperature in closed atmosphere.

2.3 Preparation of Ginger, Ajwain and KsK extract

The procedure for extract preparation is as follows; 1 g of each ginger, ajwain and Kabasura Chooranam (KSC) were weighed separately and 50 mL demineralised water was added to each container. The mixture was heated at 60 °C till its volume gets reduced to one fifth of the original volume. After that, the solution was filtered using Whatman filter paper and the resulting extract was used immediately after preparation.

3. Results and discussion

3.1 Physical characterisations

Powdered XRD pattern of the synthesized α-Fe_2O_3 is shown in Fig. 1 A. Diffraction peaks observed at (2θ) 24.24°, 33.16°, 35.93°, 40.68°, 49.39°, 54.14°, 57.70°, 62.65° and 63.84° could be assigned to (012), (104), (110), (113), (024), (116), (122), (214) and (300) Bragg reflections of the rhombohedral structure (Space group R-3c). The calculated lattice parameters $a = b = 5.0248$ Å and $c = 13.7163$ Å and unit cell volume 299.92 $Å^3$ were in good agreement with the International Centre for Diffraction Data (ICDD; Card no.:01-084-0307). Further, XRD pattern exhibited strong peak at $2\theta \sim 33°$ corresponding to (104) plane confirming hematite phase formation. Average crystallite size of

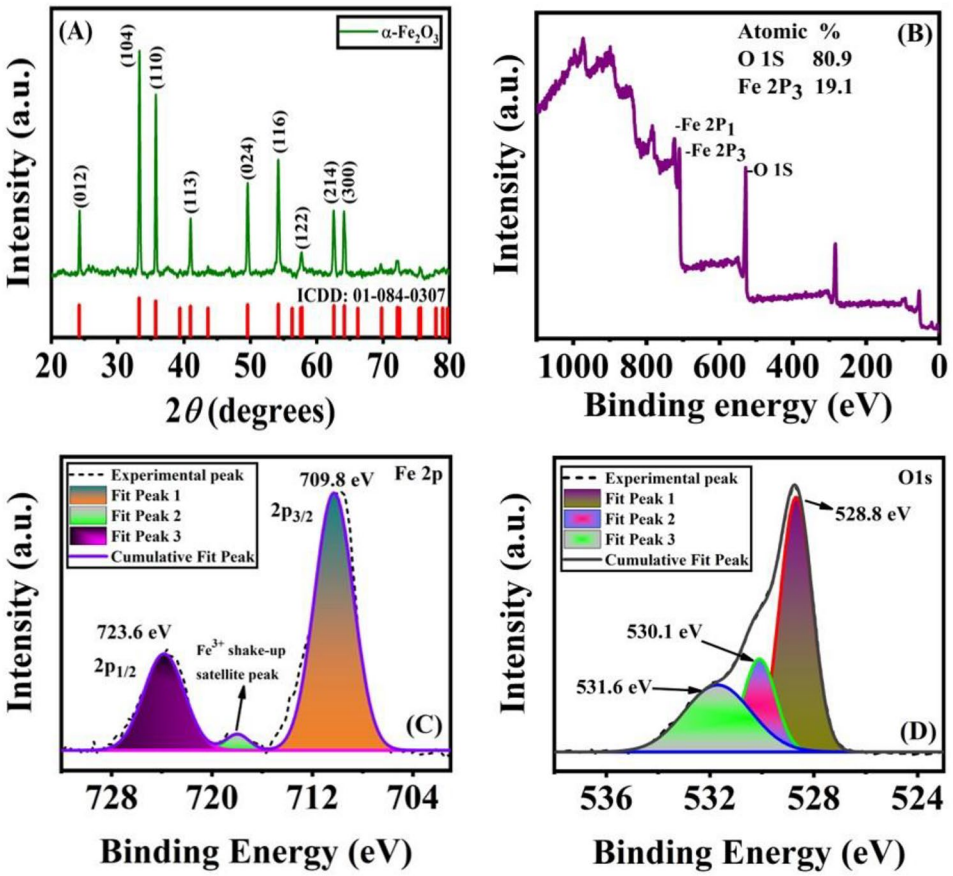

Fig. 1 (A) Powder XRD pattern of synthesized α-Fe_2O_3 nanoparticles; (B) XPS survey scan spectrum of α-Fe_2O_3 nanoparticles. (C) XPS spectra of Fe $2P_3$ and (D) XPS spectra of O1s

synthesized α-Fe_2O_3 nanoparticles was calculated as 33 nm using Debye Scherrer formula,

$(D = 0.9\ \lambda/\beta\ \cos\theta)$

Where β is the full width at half maximum (FWHM) in radian of the peak with given (hkl) value, λ = 1.5406Å of the CuKα radiation and θ is the diffracting angle.

3.2 X-ray Photoelectron Spectroscopy (XPS) analyses

The surface chemical composition and the valence states of Fe and O ions of representative α-Fe_2O_3 sample were investigated by XPS analyses and the results are shown in Fig. 1B. A survey scanning spectrum of α-Fe_2O_3 indicates that the iron and oxygen are the main constituent elements. The high-resolution Fe 2p spectrum shows two distinct peaks with binding energies of about 709.8 eV for Fe $2p_{3/2}$ and 723.6 eV for $2p_{1/2}$ and the difference in bandgap energy (13.8 eV) indicated that the iron ion exists in Fe^{3+} state in the compound. It can be noticed that the Fe $2p_{3/2}$ peak is narrower, stronger and has larger area than Fe $2p_{1/2}$ because Fe $2p_{3/2}$ has a degeneracy of four states while Fe $2p_{1/2}$ has only two in spin-orbit (j-j) coupling(Fig. 1 C).In addition to this, a small peak obtained at the binding energy of 718.6 eV is due to Fe^{3+} shake-up satellite peak of α-Fe_2O_3 nanoparticles. Oxygen will always be present on samples exposed to the atmosphere, either due to adventitious contamination, oxidation or water. To determine the presence of oxide and possible hydroxyl species in the Fe_2O_3, the O 1s spectrum was recorded as shown in Fig. 1D. The result shows three peaks with binding energy at about 528.8 eV, 530.1 eV and 531.6 eV. The peak appeared at 528.8 eV has been ascribed to lattice oxygen, confirming the oxygen valence state as 2+. The other two peaks at 530.1 eV and 531.6 eV correspond to oxygen vacancies and surface absorbed water molecules.

3.3 Transmission electron microscopic (TEM) analysis

TEM pictures have been recorded to study the morphology and structure of the α-Fe_2O_3 nanoparticles. Figure 2 A shows formation of nanosized particulates with clean surface features. It is clear that the hematite crystallites have formed as spherical and rhombohedral shaped particles with variant sizes and are well crystallized in nature. The size of nanoparticles depends largely on the growth period and concentration of precursor used in the synthesis of hematite. Average crystallite size of α-Fe_2O_3 particulates was found

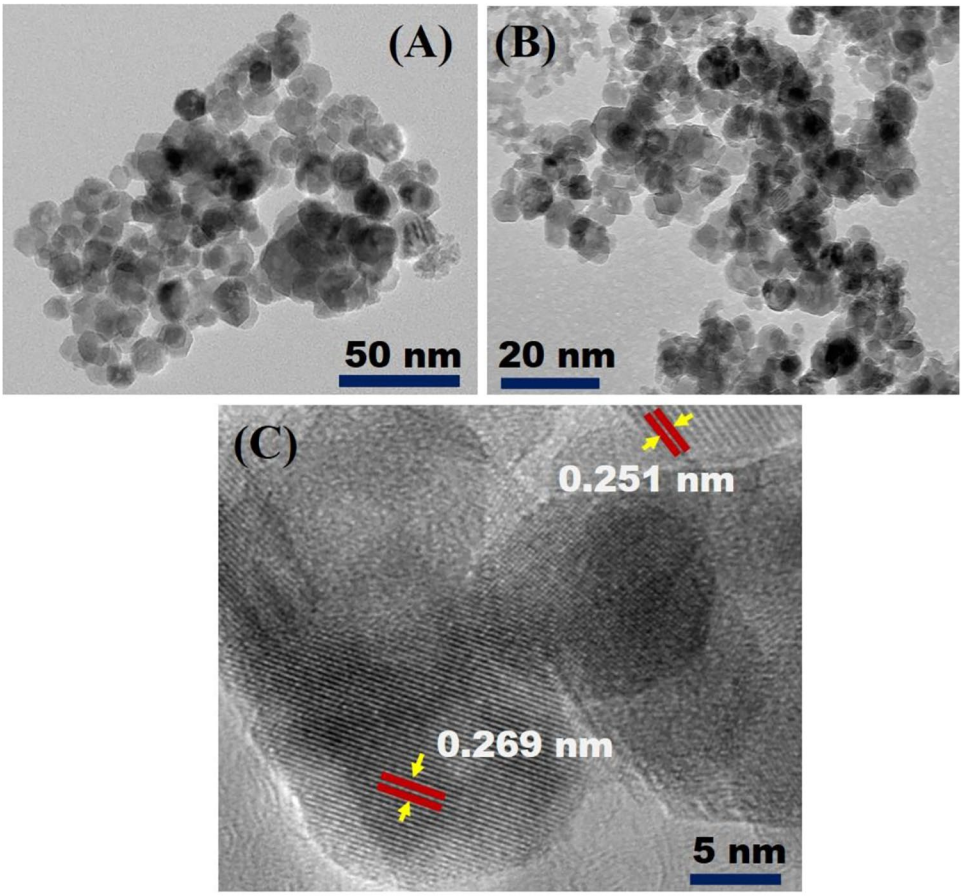

Fig. 2 (A) TEM and (B) HRTEM images of α- Fe_2O_3 nanoparticles

to be in the range of 25–33 nm, in good agreement with the powder XRD data. The size distribution was measured by 5 nm TEM image using Image J software and it obeys the logical normal distribution[27]. This result also indicates larger surface area of the synthesized Fe_2O_3 NPs, which is a desirable feature of the electrode material for sensing applications.

3.4 Electrocatalytic activity of α-Fe_2O_3 modified GCE

The electrocatalytic activity of the α-Fe_2O_3 modified GCE was studied by performing cyclic voltammetry in a redox mediator $[Fe(CN)_6]^{3-/4-}$. Figure 3 A shows the cyclic voltammograms (CVs) recorded at bare GCE and α-Fe_2O_3 modified GCE in 1 mM $[Fe(CN)_6]^{3-/4-}$ containing 0.1 M KCl at a scan rate of 50 mV/s. The bare electrode exhibited well resolved redox peaks at 0.32 V and 0.23 V whereas the α-Fe_2O_3 modified GCE showed improved catalytic activity which resulted in higher peak current (Ip_a = 18.9 µA and Ip_c = -17.69 µA) at a potential of 0.29 V and 0.19 V. The catalytic ability and increased surface area of α-Fe_2O_3 nanoparticles resulted in the improved peak current when compared to that of bare GCE.

The rate of electron transfer at the electrode-electrolyte interface was studied by electrochemical impedance spectroscopy (Fig. 3B). The results are shown in the form of Nyquist curves in which the semi-circle portion related to electron transfer limited process and a linear part resulting from the diffusion process. The charge transfer resistance (R_{CT})values for bare and α-Fe_2O_3 modified GCEs were calculated as 1450 Ω/cm^2 and 1299 Ω/cm^2 respectively. The relatively lower R_{CT} value of α-Fe_2O_3 modified GCE proves that it has higher catalytic activity and the results are in good agreement with cyclic voltammetry results.

3.5 Electrochemical behaviour of Gingerol and Thymol

The observed electrocatalytic activity of the α-Fe_2O_3 NPs suggests it as a good platform for sensing applications. The microscopic defect sites and higher surface area of the NPs lead to increased reaction sites that allow a greater number of analyte molecules to get tethered onto the electrode through which it could be detected easily. Here, the α-Fe_2O_3 NPs modified GCE has been applied for the determination of GIN and THY individually and simultaneously. Figure 3 C shows the CVs recorded at α-Fe_2O_3/GCE in 0.1 M

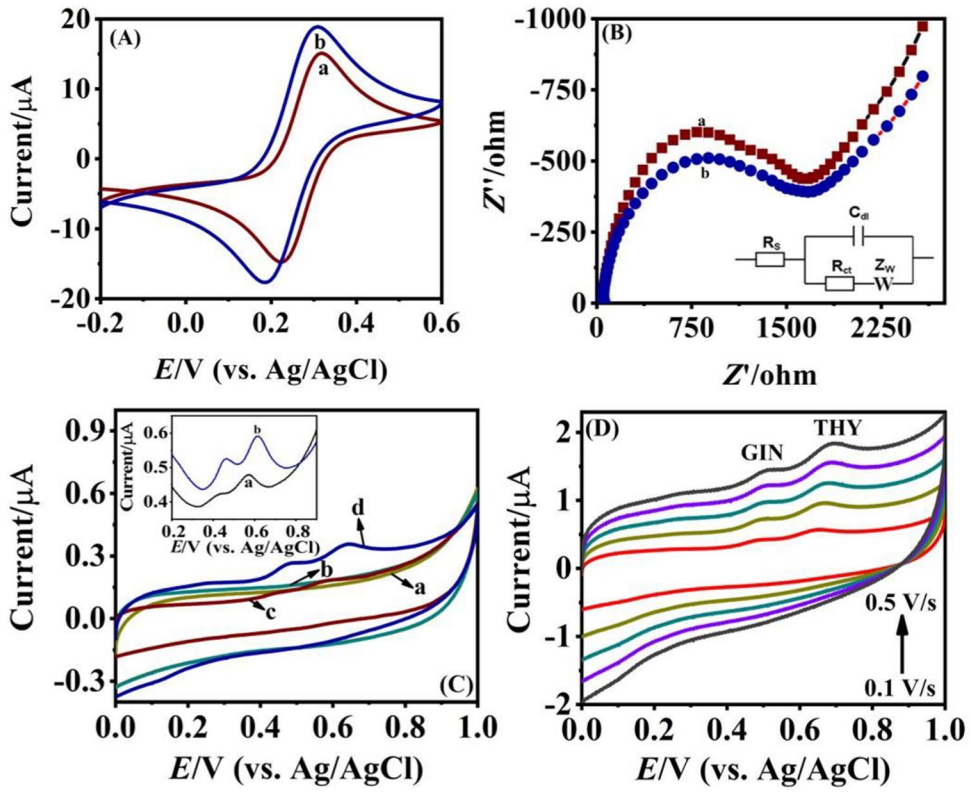

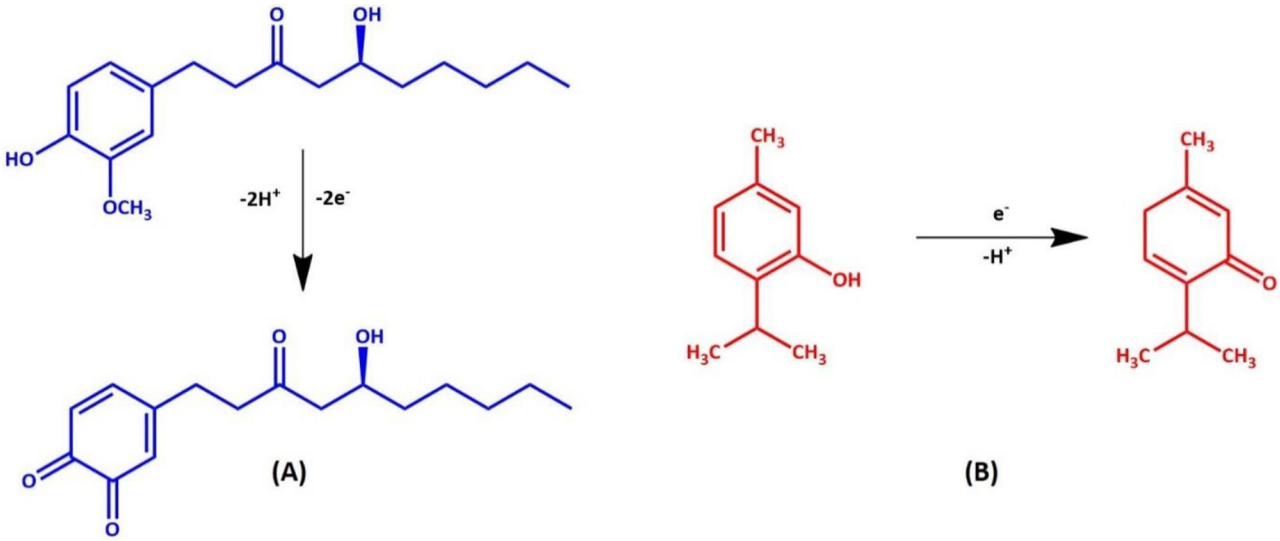

Fig. 3 (A) Cyclic voltammograms recorded at (a) bare GCE and (b) α-Fe_2O_3/GCE in 1mM $[Fe(CN)_6]^{3-/4-}$ containing 0.1 M KCl at a scan rate of 50 mV/s; (B) EIS of (a) bare GCE and (b) α-Fe_2O_3/GCE; (C) CVs recorded at (a) bare GCE and (b) α-Fe_2O_3/GCE in 0.1 M PBS (pH 7.0) containing 10 μM each GIN and THY; inset shows the SWVs of bare GCE (a) and α-Fe_2O_3/GCE (b) in 0.1 M PBS (pH7.0) containing 10 μM of each GIN and THY. (D) CVs recorded at different scan rates (0.06 V/s – 0.1 V/s) in the presence of 10 μM each GIN and THY at α-Fe_2O_3/GCE.

Fig. 4 Probable reaction mechanism for electro-oxidation of (a) Gingerol and (b) Thymol at the α-Fe_2O_3/GCE.

phosphate buffer saline (PBS; pH 7.0) in the potential window of 0 to 1.0 V at the scan rate of 0.05 V/s. In Fig. 3 C, curve *a* and curve *b* represent the CVs of bare and α-Fe_2O_3 modified GCEs in the absence of GIN and THY, whereas curve *c* and curve *d* represent the CVs recorded for bare and α-Fe_2O_3 modified GCEs in the presence of 10 μM each GIN and THY. It is observed that both the bare and α-Fe_2O_3 modified electrodes exhibit two strong peaks corresponding to oxidation of GIN and THY. At α-Fe_2O_3 modified electrode, the GIN oxidation peak was observed at 0.47 V and for THY at 0.65 V, whereas bare GCE showed at 0.45 and 0.57 V for GIN and THY respectively. Interestingly, the peak separation at α-Fe_2O_3/GCE was found to be slightly higher (0.18 V) when compared to that of bare electrode (0.12 V). In addition to this, the oxidation of GIN and THY gave higher currents (0.269 μA and 0.359 μA for GIN and THY)

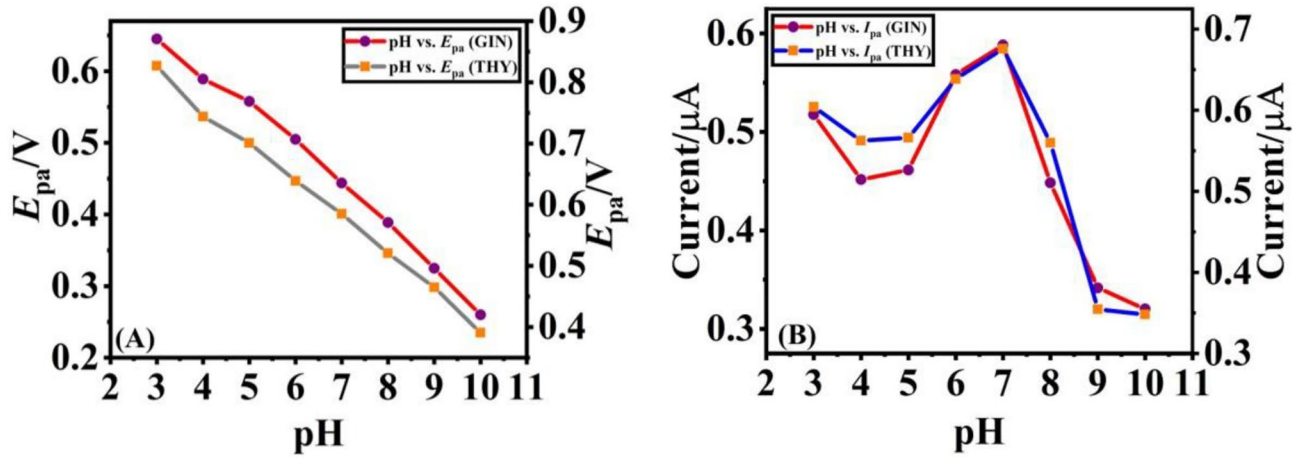

Fig. 5 (A) Plot of pH vs. Epa of GIN and THY. (B) Plot of pH vs. Ipa of GIN and THY.

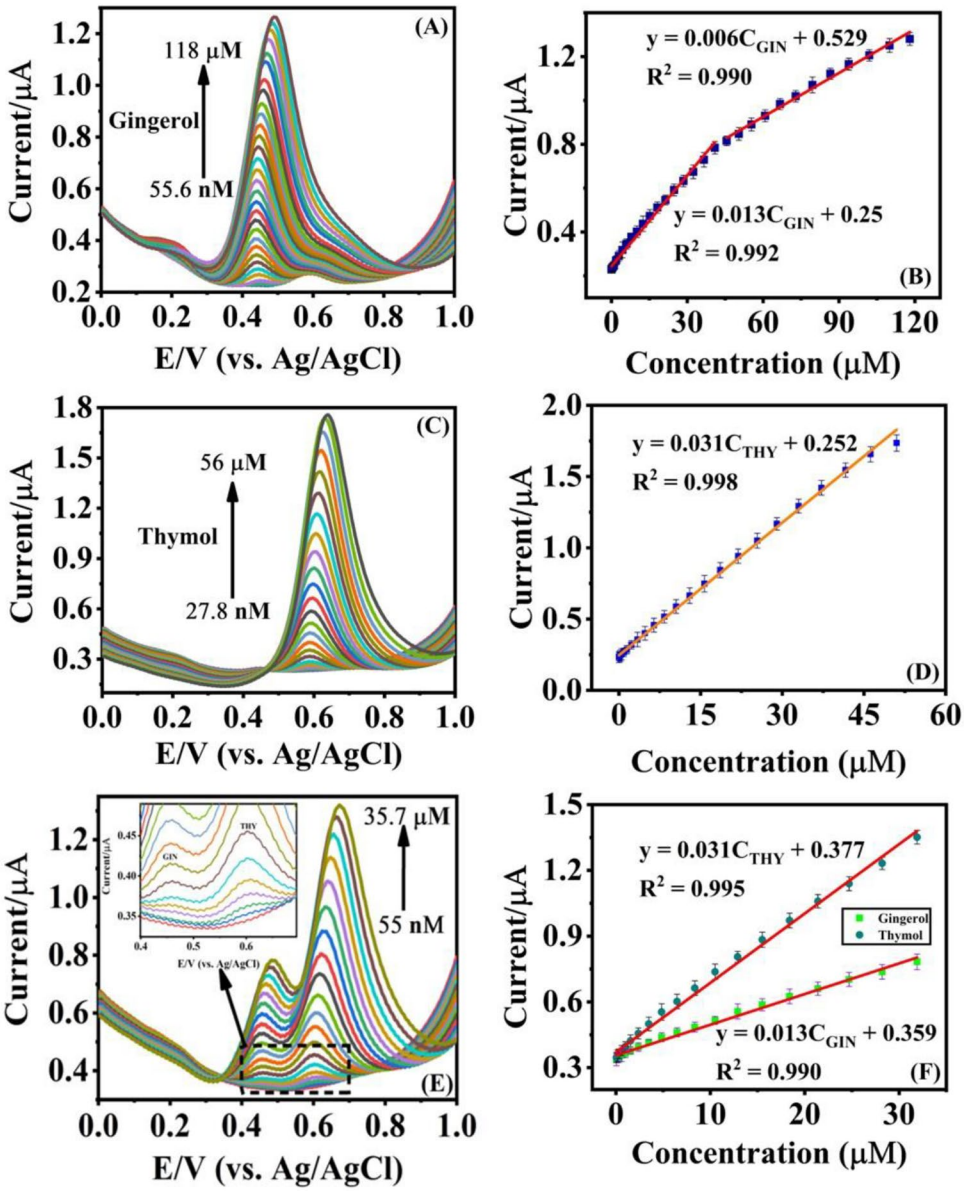

Fig. 6 (A) SWVs recorded for various concentrations of GIN (55.6 nM to 118 μM) in 0.1 M PBS (pH 7.0) at α-Fe_2O_3/GCE; (B) Plot of concentration of GIN vs. oxidation peak currents. (C) SWVs recorded for various concentrations of THY (27.8 nM to 56 μM) in 0.1 M PBS (pH 7.0) at α-Fe_2O_3/GCE. (D) Plot of concentration of THY vs. oxidation peak currents. (E) Simultaneous determination of GIN and THY at α-Fe_2O_3/GCE in various concentrations of GIN and THY (55 nM to 35.7 M). (F) Plots of concentrations of GIN and THY vs. oxidation peak currents

Table 1 Comparison of the obtained results with the previous reports in the literature

Analyte	Electrode	Method	Linear range (μM)	LOD (μM)	Potential (V)	Ref.
Thymol	CeO_2/GN/GCE	DPV	0.1–18	0.05	0.467	[8]
	CeO_2/Brij35/GCE	DPV	0.7–10.1	20	0.59	[11]
	SWCNTs/SPEs	DPV	5–90	4	0.045	[12]
	Ag@c@Ag/GCE	DPV	0.1–10	0.0216	0.86	[28]
	GCE	LSV	85–1300	79	1.29	[31]
	BDD electrode	SWV	4–100	3.9	1.13	[32]
	PAM@G-MIP	DPV	0.5–300	0.043	0.72	[33]
		HPLC-UV	0.40–5000 ng mL^{-1}	0.042 ng mL^{-1}		[34]
	α-Fe_2O_3	**SWV**	**0.0278–56**	**0.024**	**0.65**	**This work**
Gingerol	MWCNT-BPPG electrode	AdsSV	1–50	0.71	0.43	[3]
		RP-HPTLC	50–600 ng/band	16.84 ng/band		[34]
	α-Fe_2O_3	**SWV**	**0.0556–118**	**0.0352**	**0.47**	**This work**

than that of bare electrode with 0.126 μA and 0.185 μA for GIN and THY respectively. The plausible mechanism for electrochemical reaction of Gingerol[3] and Thymol[28] at the α-Fe_2O_3 modified GCE is shown in Fig. 4. The outstanding catalytic ability of the α-Fe_2O_3 NPs towards oxidation of GIN and THY could be due to its physical origin such as high surface area and increased number of reactive sites.

Figure 3D shows the effect of scan rate on the oxidations of GIN and THY at the α-Fe_2O_3/GCE. The oxidation peak currents were found to increase linearly with the increase of scan rate from 0.06 V/s to 0.1 V/s which confirms that the electrode process is diffusion-controlled nature. Square wave voltammetry responses of GIN and THY at the α-Fe_2O_3/GCE were recorded in 0.1 M PBS (pH 7.0) (Insert of Fig. 3 C). The results are in good agreement with the results obtained from cyclic voltammetric studies and this confirms that the modified electrode could be used effectively towards the determination of gingerol and thymol.

3.6 Effect of pH on the oxidations of Gingerol and Thymol

The results of the influence of pH on the oxidation of GIN and THY at the α-Fe_2O_3/GCE are shown in Fig. 5. It is clear from the result that the oxidations depend on pH of the PBS. At a lower pH of 3, both GIN and THY get oxidised at higher potentials of 0.64 and 0.83 V respectively. While increasing pH from 3 to 10, the oxidation peak potentials of GIN and THY got shifted to lower potentials which confirmed the participation of H^+ on the oxidation reaction at the surface of α-Fe_2O_3/GCE. Moreover, a good linear relationship between pH and $E_{p.a.}$ was obtained (Fig. 5 A) with the slope values of 0.058 for GIN and 0.059 for THY indicating one electron oxidation processes in both the cases. The oxidation peak currents increased with the increase of pH and attained a maximum at pH 7.0 and got decreased for higher pH value from 8 to 10 (Fig. 5B). Based on these results, pH 7.0 was chosen for further studies.

3.7 Selective determinations of Gingerol and Thymol

The capability of the modified electrode to determine the GIN selectively in the presence of 10 μM THY was studied by performing SWVs in 0.1 M PBS (pH 7.0). The concentration of GIN was varied from 55.6 nM to 118 μM at α-Fe_2O_3/GCE and the corresponding oxidation peak currents increased linearly with each increment of GIN (Fig. 6 A). The concentration of GIN was plotted against the oxidation peak currents which showed two linear segments of 55.6 nM to 45.6 μM and 50.4 μM to 118 μM (Fig. 6B). The regression equations for both the segments were deduced as:

I_{GIN} (μA) = 0.013C_{GIN} + 0.25 (R^2 = 0.992) (0.0556 μM – 45.6 μM).

I_{GIN}(μA) = 0.006C_{GIN} + 0.529 (R^2 = 0.990) (45.6 μM – 118 μM).

Similarly, selective determination of THY was performed at α-Fe_2O_3/GCE in 0.1 M PBS (pH 7.0) in the presence of 10 μM of GIN. The oxidation peak currents were noted after each addition of THY in the concentration range of 27.8 nM to 56 μM. A linear response was observed in the plot of concentration of THY versus current which is shown in Fig. 6 C and 6D. The regression equation was reckoned as follows;

I_{THY} (μA) = 0.031C_{THY} + 0.252 (R^2 = 0.997) (0.0278 μM – 56 μM).

The lowest detection limits (LOD) of the sensor towards selective determination of GIN and THY were calculated from the corresponding calibration curves using the formula[29].

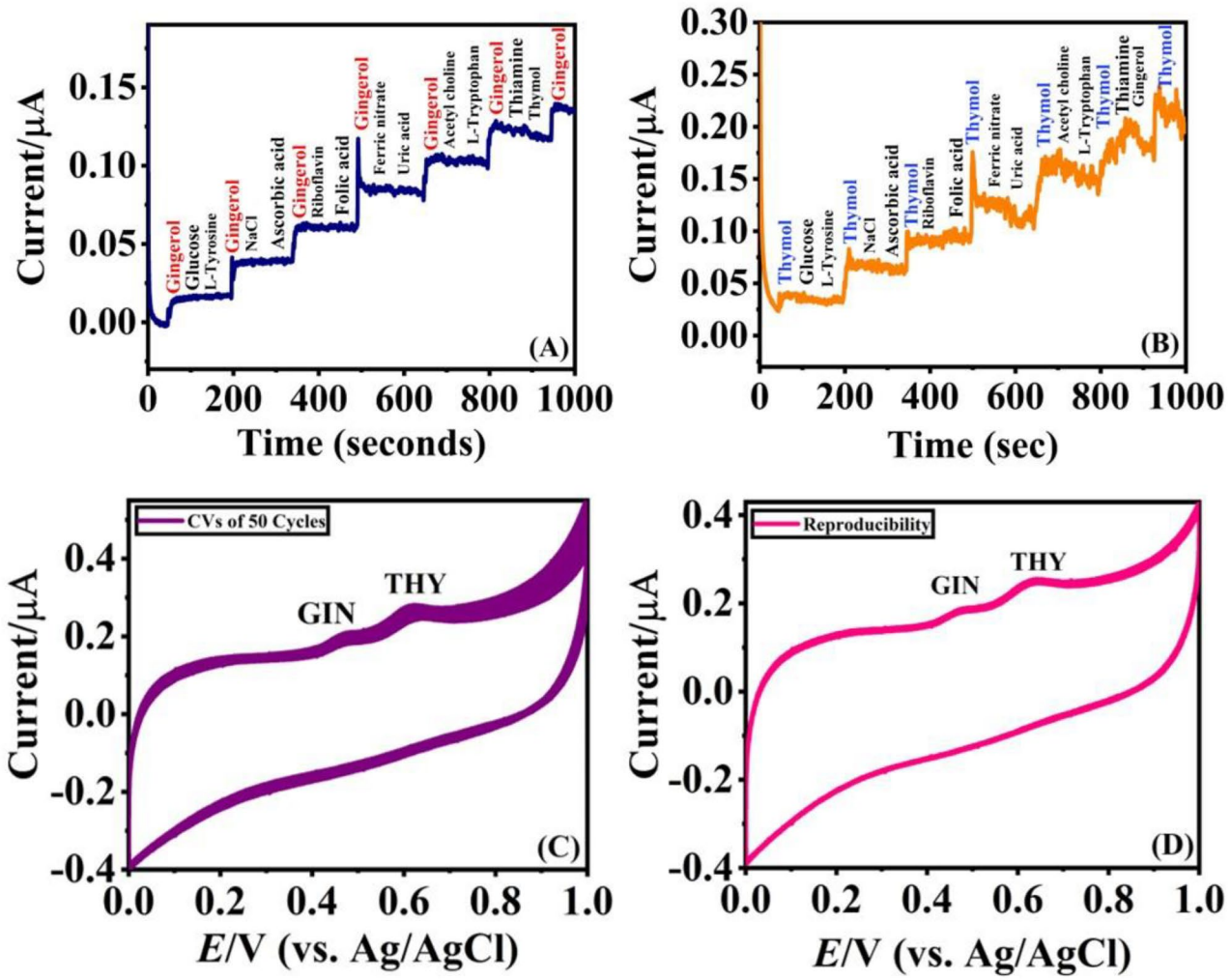

Fig. 7 (A) & (B) Amperometric responses of α-Fe_2O_3/GCEs for the addition of 10 μM of GIN and THY with successive additions of (a) Glucose, (b) L-Tyrosine, (c) NaCl, (d) Ascorbic acid, (e) Riboflavin, (f) Folic acid, (g) Ferric nitrate, (h) Uric acid, (i) Acetyl choline, (j) L-Tryptophan, (k) Thiamine, (l) Thymol in 0.1 M PBS (pH 7.0 (C) CVs of 50 cycles recorded at α-Fe_2O_3/GCE in 0.1 M PBS containing 10 μM each of GIN and THY at a scan rate of 50 mV/s.; (D) CVs recorded at ten different α-Fe_2O_3/GCEs in 0.1 M PBS containing 10 μM of each GIN and THY.

$$\text{LOD} = \frac{3 \text{ x Standard deviation}}{\text{Slope}}$$

Thus, the LODs were deduced as 35.2 nM and 24 nM for GIN and THY respectively using slope of their calibration curves. The α-Fe_2O_3/GCE displayed an impressive catalytic activity towards the oxidation of GIN and THY without requiring any additive or mediator. Table 1 shows the obtained results in comparison with the previously reported values. It can be noticed that there are only four reports published so far and the authors have employed carbon nanostructures (MWCNTs, GN, SWCNTs) and Brij35 along with metal oxides (CeO_2) to improve the sensing characteristics of the electrode. On the other hand, we have used a simple, abundantly available, and low-cost α-Fe_2O_3 as an electrode material for sensing applications which also yielded excellent results in comparison to the previous reports. The fabricated electrochemical sensor based on α-Fe_2O_3/GCE can thus be used for determination of gingerol and thymol over a wider dynamic range with the lowest detection limits.

3.8 Simultaneous determinations of Gingerol and Thymol

To explicate the ability of the modified electrode to determine the GIN and THY simultaneously, the SWVs were performed in the potential range of 0.0 to 1.0 V in 0.1 M PBS (pH 7.0). Different concentrations of GIN and THY were added simultaneously in the range of 55 nM to 35.7 μM and the resulting voltammograms were recorded (Fig. 6E).

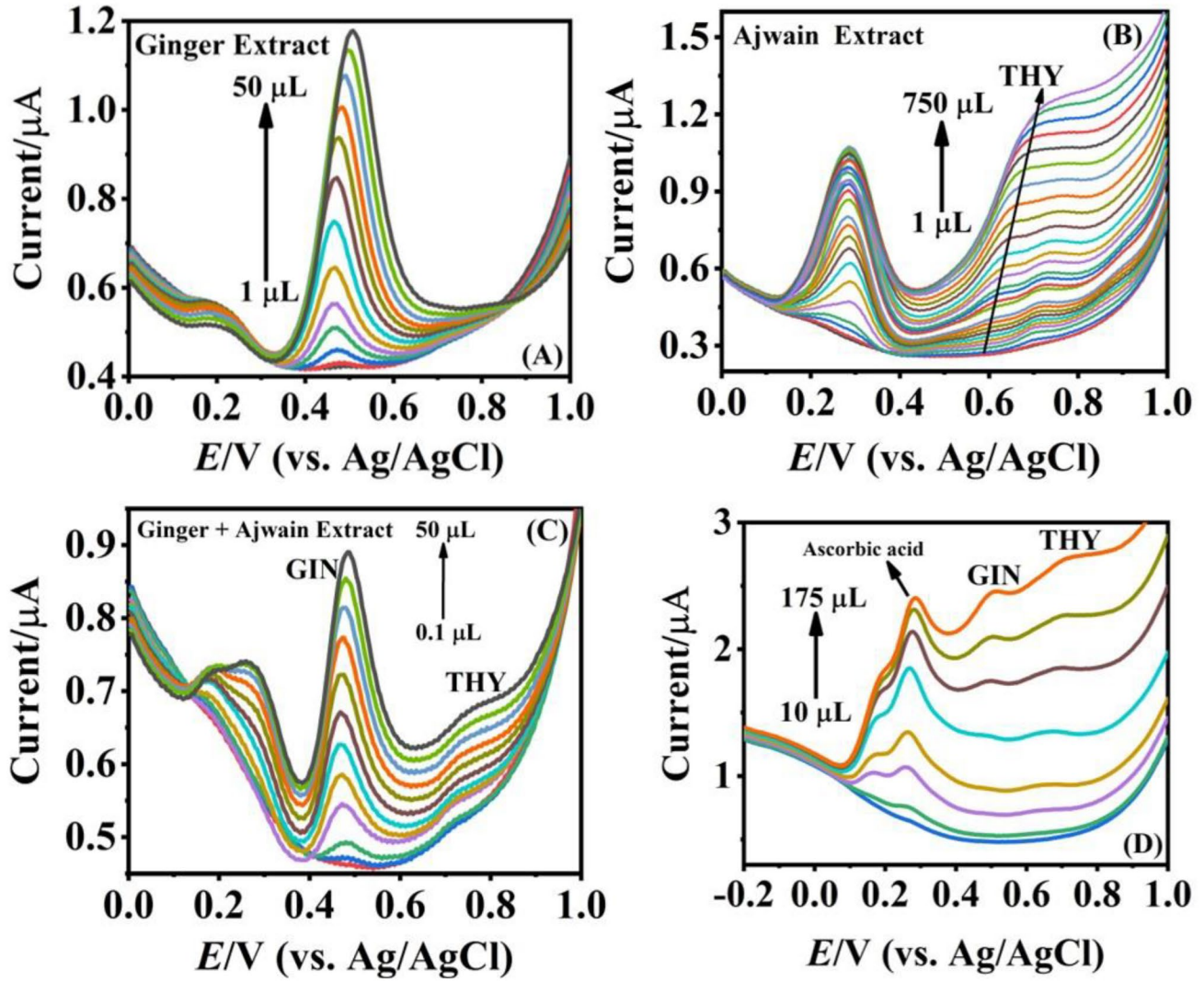

Fig. 8 (A) SWVs obtained at α-Fe_2O_3/GCE for Ginger and (B) Ajwain extracts in 0.1 M PBS (pH 7.0); (C) SWVs obtained at α-Fe_2O_3/GCE in the binary mixture containing Ginger and Ajwain extracts in 0.1 M PBS (pH 7.0). (D) SWVs obtained α-Fe_2O_3/GCE for Kabasura Kudineer in 0.1 M PBS (pH 7.0)

It could be observed that the oxidation peak currents of GIN and THY increase systematically for every addition of the analytes till they reach saturation. The oxidation peak for GIN was found at 0.46 V for the minimum concentration of 55 nM and at the maximum concentration, the peak was observed at 0.48 V with a negative potential shift of 0.02 V. In case of THY, the oxidation peak was observed at 0.6 V for minimum concentration and at 0.67 V for higher concentration of 35.7 µM. These slightly positive shifts in the oxidation potentials at higher concentrations might be due to the adsorption of oxidation products at the electrode surface during the reaction. The results further indicate that the separation between oxidation potentials of the two analytes is 190 mV at higher concentrations which is sufficient for the simultaneous sensing of GIN and THY in the binary mixtures. Moreover, it was noted that the oxidation peaks of THY were stronger compared to that of GIN for the same concentration. The peak currents were plotted against the concentrations which showed a good linearity (Fig. 6 F) and the corresponding regression equations of GIN and THY were deduced as follows;

I_{GIN} (µA) = 0.013C_{GIN} + 0.359 (R^2 = 0.990) (0.055 µM – 35.7 µM).

I_{THY} (µA) = 0.031C_{THY} + 0.377 (R^2 = 0.995) (0.055 µM – 35.7 µM).

The LODs were calculated as 34.6nM and 22nM for GIN and THY respectively. It was noticed that the LODs obtained for simultaneous detection are nearly equivalent to that of the results obtained for individual measurements. The results clearly indicate that the fabricated sensor shall

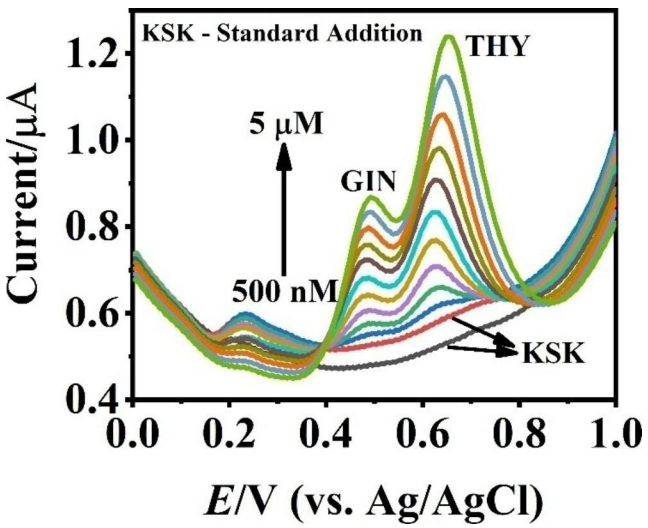

Fig. 9 SWVs obtained at α-Fe_2O_3/GCE from Kabasura Kudineer sample by standard addition method in 0.1 M PBS (pH 7.0)

NaCl, Ascorbic acid, Riboflavin, Folic acid, Ferric nitrate, Uric acid, Acetyl choline, L-Tryptophan, Thiamine and Thymol. Interestingly, the presence of excessive amounts of interferents has no effect on the oxidation of GIN at α-Fe_2O_3/GCE. Similarly, the interference ability of the electrode for THY was tested under identical conditions (Fig. 7B). As expected, the electrode displayed a better anti-interference ability without any changes in the oxidation peak currents of THY.

The stability of the α-Fe_2O_3 modified electrode was tested by cycling the electrode for about 50 cycles between potential range 0.0 to 1.0 V in 0.1 M PBS (pH 7.0) containing 10 µM of each GIN and THY (Fig. 7 C). The current responses for the oxidations of THY and GIN decreased to a small extent with an RSD value of 9.9% and 9.18% for GIN and THY respectively confirming the stability of the fabricated electrode towards the simultaneous determinations.

The reproducibility of the modified electrode was studied by performing CVs of ten repetitive measurements in 0.1 M PBS (pH 7.0) containing 10 µM of each GIN and THY (Fig. 7D). The modified electrode displayed almost same response at all the ten measurements with an RSD value of 1.08% and 0.97% GIN and THY respectively. The obtained results proved that the electrode possesses excellent reproducibility and that the electrode is highly suitable for the simultaneous determination of GIN and THY.

Table 2 Determination of GIN and THY in KsK sample using fabricated electrode (n = 3)

Sample	Analyte	Spiked (µM)	Initial (µM)	Expected (µM)	Detected (µM)	Recovery (%)	RSD (%)
KsK extract	**GIN**	0	0	0	0.37	-	1.32
		0.5	0.37	0.87	0.89	102.2	1.61
		1	0.87	1.87	1.82	97.3	1.92
		1.5	1.87	3.37	3.41	101.1	0.83
		2	3.37	5.37	5.35	99.6	0.26
		3	5.37	8.37	8.32	99.4	0.42
		4	8.37	12.37	12.42	100.4	0.29
		5	12.37	17.37	17.40	100.1	0.12
	THY	0	0	0	0.44	-	0.81
		0.5	0.44	0.94	0.97	103.1	2.22
		1	0.94	1.94	1.99	102.5	1.8
		1.5	1.94	3.44	3.48	101.1	1.42
		2	3.44	5.44	5.47	100.5	0.39
		3	5.44	8.44	8.39	99.4	0.42
		4	8.44	12.44	12.41	99.7	0.17
		5	12.44	17.44	17.48	100.2	0.16

be useful for the simultaneous detection and quantification of Gingerol and Thymol, the phytochemicals of food and medicinal importance.

3.9 Interference, Stability and Repeatability of the modified electrode

The ability of the modified electrode to determine the GIN and THY selectively in the presence of several potential interferents was tested using sensitive chronoamperometric technique. Figure 7 A shows the anti-interference property of the electrode for GIN determination in the presence of 50-fold excess of interferents such as Glucose, L-Tyrosine,

3.10 Detection of GIN and THY in Ginger and Ajwain

Ginger and Ajwain extracts, the major sources for Gingerol and Thymol were prepared independently and used as real samples to test efficacy of the fabricated sensor.

SWVs recorded for ginger extract in PBS (pH 7.0) exhibited a strong oxidation peak at about 0.43 V confirming the presence of gingerol (Fig. 8 A). Similarly, ajwain extract showed a peak at 0.67 V corresponding to the oxidation of Thymol(Fig. 8B). Different volumes of ginger and ajwain extracts were added to PBS (pH 7.0) and the resulting voltammograms were recorded. The obtained results have been compared with the standard samples(Fig. 6) and the amount of GIN and THY present in the ginger and ajwain extract were deduced as 2.3 mg/mL and 0.7 mg/mL respectively. In another set of experiments, the binary mixture of ginger and ajwain extracts was prepared by mixing equal amounts (0.5 g each in 50 mL of water) and voltammetric measurements were performed in PBS for various concentrations of the mixed solution (Fig. 8 C). The obtained results (Fig. 8) were in good agreement with the results of individual measurements for GIN and THY and the amounts were deduced as 1.5 mg/mL and 0.48 mg/mL for GIN and THY respectively.

3.11 Determination of GIN and THY in Traditional Medicine

In order to identify and quantify the GIN and THY content in the traditional Sidha medicine called Kabasura Kudineer (KsK), square wave voltammograms were recorded for different concentrations of KsK in the range of 10 µL to 175 µL (Fig. 8D). The peaks corresponding to GIN and THY were observed at 0.49 and 0.69 V respectively. In order to ensure this result, the standard addition method was performed by adding known amount of GIN and THY to the KsK extract at α-Fe_2O_3/GCE in PBS (7.0) and the results were shown in Fig. 9. The peaks corresponding to GIN and THY oxidation were found to increase linearly with the addition of commercial GIN and THY. The amount of GIN and THY present in the KsK extract was calculated by the following formula[30]:

$$\frac{\text{Concentration in KsK}}{\text{Concentration in spiked sample}} = \frac{\text{Oxidation peak current of KsK}}{\text{Oxidation peak current of spiked sample}}$$

The results indicate that the modified electrode displayed an excellent result with good recovery percentage. Moreover, it is also proved that there is no matrix effect at the electrode with good accuracy. The calculated values of GIN and THY present in the KsK extract were shown in (Table 2). The average RSDs of GIN and THY were estimated as 0.84% and 0.92% respectively; and the recovery percentages of GIN and THY were calculated as 100.01% and100.92% respectively, which indicate the suitability of the fabricated sensor for determination of the chosen analytes.

4 Conclusion

In this work, a new electrochemical sensor was fabricated using α-Fe_2O_3 nanoparticles for the simultaneous determination of Gingerol and Thymol for the first time. The synthesised α-$Fe_2O_3$was characterised by XRD, XPS and TEM and its electrocatalytic properties of was studied by CV and EIS. The sensors exhibited an excellent catalytic activity towards gingerol and thymol with a wider working range of 55.6 nM to 118 µM for GIN and 27.8 nM to 56 µM for THY respectively. Moreover, the LODs of the sensor was found to be high (35.2 nM for GIN and 24 nM for THY) when compared to the previously reported values. The practical utility of the fabricated sensor to determine gingerol and thymol in real samples such as Kabasura Kudineer, ginger extract and ajwain extract was demonstrated. High stability, good reproducibility and selectivity of the fabricated sensor makes it suitable for applications in the food and pharmaceutical industries.

Acknowledgements Authors acknowledge CSIR (No. 03(1419)/18/EMR-II dated: 04.06.2018) and MHRD-RUSA 2.0 (No. F.24–51/2014-U, Policy (TN-Multi-Gen), dated: 09.10.2018), DST-PURSE Phase 2/38(G) dated: 21.02.2017) for financial assistance.

Declarations

Statements and declarations The authors declare that they have no known competing financial interests or personal relationships that could have appeared to influence the work reported in this paper.

References

1. A.T. Mbaveng, V. Kuete, *Zingiber Officinale* (Elsevier Inc., 2017)
2. B.J. Oso, A.O. Adeoye, I.F. Olaoye, J. Biomol. Struct. Dyn. **40**, 389 (2022)
3. K. Chaisiwamongkhol, K. Ngamchuea, C. Batchelor-Mcauley, R.G. Compton, Analyst **141**, 6321 (2016)
4. A. Bhaskar, A. Kumari, M. Singh, S. Kumar, S. Kumar, A. Dabla, S. Chaturvedi, V. Yadav, D. Chattopadhyay, and V. Prakash Dwivedi, Int. Immunopharmacol. **87**, 106809 (2020)
5. L. Lei, Y. Liu, X. Wang, R. Jiao, K.Y. Ma, Y.M. Li, L. Wang, S.W. Man, S. Sang, Y. Huang, Z.Y. Chen, J. Agric. Food Chem. **62**, 10515 (2014)
6. A.I. Foudah, F. Shakeel, H.S. Yusufoglu, S.A. Ross, P. Alam, Foods 9, (2020)
7. J.B. Weon, H.J. Yang, J.Y. Ma, C.J. Ma, J. Nat. Med. **66**, 510 (2012)
8. X. Zhao, Y. Du, W. Ye, D. Lu, X. Xia, C. Wang, New. J. Chem. **37**, 4045 (2013)
9. S.Y. Li, Y.J. Ru, M. Liu, B. Xu, A. Péron, X.G. Shi, Livest. Sci. **145**, 119 (2012)
10. M. Alagiri, S.B.A. Hamid, J. Sol-Gel Sci. Technol. **74**, 783 (2015)
11. G. Ziyatdinova, E. Ziganshina, P.N. Cong, H. Budnikov, Food Anal. Methods **10**, 129 (2017)
12. F.G. Fuentes, M.ÁL. Gil, S. Mendoza, A. Escarpa, Electroanalysis **23**, 2212 (2011)

13. Z. Dabirifar, S. Khadempir, A. Kardan, C. Karaman, Chem. Eng. Res. Des. **180**, 38 (2022)
14. S. Korkmaz, A. Kariper, O. Karaman, C. Karaman, Ceram. Int. **47**, 34514 (2021)
15. İA. Kariper, S. Korkmaz, C. Karaman, O. Karaman, Fuel **324**, 124497 (2022)
16. M. Alizadeh, E. Demir, N. Aydogdu, N. Zare, F. Karimi, S.M. Kandomal, H. Rokni, Y. Ghasemi, Food Chem. Toxicol. 163, (2022)
17. M. Ghalkhani, N. Zare, F. Karimi, C. Karaman, M. Alizadeh, Y. Vasseghian, Food Chem. Toxicol. 161, (2022)
18. J.A. Buledi, N. Mahar, A. Mallah, A.R. Solangi, I.M. Palabiyik, N. Qambrani, F. Karimi, Y. Vasseghian, and H. Karimi-Maleh, Food Chem. Toxicol. **161**, (2022)
19. P. Nasehi, M.S. Moghaddam, N. Rezaei-savadkouhi, M. Alizadeh, M.N. Yazdani, H. Agheli, J. Food Meas. Charact. **16**, 2440 (2022)
20. A.C. Anithaa, S.B. Mayil Vealan, G. Veerapandi, C. Sekar, J. Appl. Electrochem. **51**, 1741 (2021)
21. A.C. Anithaa, S.B. Mayil Vealan, and S. C., Sensors Actuators A Phys. 331, (2021)
22. G. Veerapandi, S. Meenakshi, S. Anitta, C. Arul, P. Ashokkumar, C. Sekar, Food Chem. 382, (2022)
23. N. Lavanya, E. Fazio, F. Neri, A. Bonavita, S.G. Leonardi, G. Neri, C. Sekar, J. Electroanal. Chem. **770**, 23 (2016)
24. S. Meenakshi, S. Anitta, A. Sivakumar, S. A. Martin Britto Dhas, and C. Sekar, Microchem. J. **168**, (2021)
25. P.T. Bhattacharya, S.R. Misra, M. Hussain, Scientifica (Cairo). 2016, (2016)
26. L. Gao, K. Fan, X. Yan, Theranostics **7**, 3207 (2017)
27. J.C. Wang, J. Ren, H.C. Yao, L. Zhang, J.S. Wang, S.Q. Zang, L.F. Han, Z.J. Li, J. Hazard. Mater. **311**, 11 (2016)
28. T. Gan, Z. Lv, Y. Deng, J. Sun, Z. Shi, Y. Liu, New. J. Chem. **39**, 6244 (2015)
29. M.E. Swartz, I.S. Krull, in Handb. Anal. Valid. (2012)
30. A.M. Fekry, M. Shehata, S.M. Azab, A. Walcarius, Sens. Actuators B Chem **302**, 127172 (2020)
31. S.N. Robledo, G.D. Pierini, C.H.D. Nieto, H. Fernández, M.A. Zon, Talanta **196**, 362 (2019)
32. D.M. Stanković, Anal. Biochem. **486**, 1 (2015)
33. H. Naskar, S. Biswas, B. Tudu, R. Bandyopadhyay, P. Pramanik, IEEE Sens. J. **19**, 8583 (2019)
34. E. Kasiri, H. Haddadi, H. Javadian, A. Asfaram, J. Chromatogr. B Anal. Technol. Biomed. Life Sci. **1182**, 122941 (2021)

Authors and Affiliations

G. Veerapandi[1] · S. Meenakshi[1] · C. Sekar[1]

✉ C. Sekar
Sekar2025@gmail.com

[1] Department of Bioelectronics and Biosensors, Alagappa University, 630 004 Karaikudi, Tamilnadu, India